JOURNAL OF GEOPHYSICAL RESEARCH: SPACE PHYSICS, VOL. 118, 2809–2823, doi:10.1002/jgra.50342, 2013

Upstream ultra-low frequency waves in Mercury's foreshock region: MESSENGER magnetic field observations

Guan Le,[1] Peter J. Chi,[1,2] Xochitl Blanco-Cano,[3] Scott Boardsen,[1] James A. Slavin,[4] Brian J. Anderson,[5] and Haje Korth[5]

Received 8 January 2013; revised 13 May 2013; accepted 15 May 2013; published 7 June 2013

[1] Mercury's bow shock is unique in our solar system as it is produced by low Mach number solar wind blowing over a small magnetized body. The availability of MESSENGER orbiter data enables us for the first time to conduct an in-depth study of upstream waves in Mercury's foreshock. This paper reports first results of an observational study of upstream ULF waves in Mercury's foreshock using high-time resolution magnetic field data from the MESSENGER spacecraft to understand the general morphology of these waves. We find that the most common wave phenomenon in Mercury's foreshock has frequencies ~ 2 Hz, with properties similar to the 1 Hz whistler waves in the Earth's foreshock. Their generation appears to be generic to the shock and not affected by the weak strength and small size of Mercury's bow shock. On the other hand, the most common wave phenomenon in the Earth's foreshock is the large-amplitude 30 second waves, identified as fast magnetosonic waves generated by backstreaming ions. Similar waves at Mercury have wave frequencies at ~ 0.3 Hz, but occur only sporadically. The general lack of strong "30 second" magnetosonic waves at Mercury can be attributed to the lack of strong backstreaming ions due to a weak bow shock and not enough time for wave growth due to the small foreshock size. Superposed on the "1 Hz" whistler waves, there are short bursts of spectral peaks at ~ 0.8 Hz that are new and have not been reported previously in Mariner 10 data.

Citation: Le, G., P. J. Chi, X. Blanco-Cano, S. Boardsen, J. A. Slavin, and B. J. Anderson (2013), Upstream ultra-low frequency waves in Mercury's foreshock region: MESSENGER magnetic field observations, *J. Geophys. Res. Space Physics*, *118*, 2809–2823, doi:10.1002/jgra.50342.

1. Introduction

[2] The foreshock is the spatially asymmetric region magnetically connected to the planetary bow shock. It contains backstreaming charged particles from the bow shock, produced by either reflection of solar wind particles at the bow shock or leakage of shocked plasma from downstream of the shock [e.g., *Thomsen et al*., 1983]. The backstreaming particles in the foreshock move upstream along the interplanetary magnetic field (IMF) and provide a source of free energy for various plasma instabilities as they move upstream against the incoming solar wind flow. Upstream waves refer to all types of electromagnetic and electrostatic waves generated by the backstreaming particles in the foreshock. The study of foreshocks other than the Earth's is important for extending our understanding of collisionless shocks and foreshock physics since the bow shock strength varies with heliocentric distance from the Sun, and the sizes of the bow shocks are different at different planets. Upstream waves have been observed in the foreshock regions of all the planets that have been visited by spacecraft as well as in front of cometary bow shocks and interplanetary shocks. While upstream waves have been studied in depth in the Earth's foreshock, our knowledge of Mercury's upstream waves is rather poor because it came exclusively from the magnetic field data during the Mercury flybys of Marnier 10, the only spacecraft which has encountered the planet before MESSENGER was launched [*Fairfield and Behanon*, 1976]. The magnetic field data from MESSENGER orbiting spacecraft open up a door for an in-depth exploration of upstream waves at Mercury.

[3] Although there are many similarities between Mercury's foreshock and Earth's foreshock, they differ in several aspects: the size and the strength of the bow shock as well as the value of the solar wind Mach number at the two planets. Mercury's bow shock is unique in our solar system as it is produced by low Mach number solar wind blowing over a small magnetized body with a predominately radial interplanetary magnetic field. Mercury is the smallest of the terrestrial planets. Mariner 10 first

[1]Space Weather Laboratory, Heliophysics Science Division, NASA Goddard Space Flight Center, Greenbelt, Maryland, USA.
[2]Institute of Geophysics and Planetary Physics, University of California, Los Angeles, California, USA.
[3]UNAM, Instituto de Geofisica, Mexico City, Mexico.
[4]Department of Atmospheric, Oceanic and Space Sciences, University of Michigan, Ann Arbor, Michigan, USA.
[5]The Johns Hopkins University Applied Physics Laboratory, Laurel, Maryland, USA.

Corresponding author: G. Le, NASA Goddard Space Flight Center, Code 674, Greenbelt, MD 20771, USA. (Guan.Le@nasa.gov)

2169-9380/13/10.1002/jgra.50342

established and MESSENGER confirmed that Mercury has an intrinsic magnetic field and the magnetic moment is only about 4×10^{-4} of that of the Earth [*Ness et al*., 1975; *Russell et al*., 1988; *Anderson et al*., 2008]. The weak magnetic moment, combined with a large solar wind dynamic pressure at the planet, results in a very small planetary magnetosphere, in both absolute value and relative to the planet. Although Mercury's magnetosphere can form a magnetic cavity to shield the solar wind from the planet and divert the solar wind flow around it in a manner similar to the Earth's magnetosphere, the bow shock formed in front of the magnetic cavity is both very weak due to the low solar wind Mach number and very small in dimension (~ 1/10 of the Earth's bow shock). In addition, the solar wind is unique at Mercury: the Mach number is low and the IMF direction is frequently near the radial direction. *Slavin and Holzer* [1981] list typical interplanetary conditions and bow shock parameters at Mercury and the Earth. The typical Alfvénic Mach number ranges from ~ 4 to 6, and the magnetosonic Mach number ~ 5–6 at Mercury. In comparison, the typical Alfvénic and magnetosonic Mach numbers at the Earth are ~ 9 and 7, respectively. The IMF Parker spiral angle is ~ 20° at Mercury and ~ 45° at the Earth. We do expect that there are similarities and differences among the upstream waves in Mercury's foreshock and the Earth's foreshock.

[4] To our knowledge, there are only a few publications focusing on the topic of upstream waves at Mercury, all reporting in situ observations by Mariner 10. *Fairfield and Behannon* [1976] first reported Mariner 10 observations and classified Mercury upstream waves into two classes that appear to correspond to two types of upstream waves at Earth: (1) lower-frequency (~ 5–10 s), large-amplitude waves similar to the 30 second waves at Earth that occur in the region upstream from quasi-parallel shocks [*Greenstadt et al*., 1968]; and (2) higher-frequency (~ 2 Hz), small-amplitude waves similar to the 1 Hz waves at Earth that occur upstream from both quasi-parallel and quasi-perpendicular shocks [*Fairfield*, 1974]. Such classifications of Mercury upstream waves were based on the wave properties and their frequency characteristics. *Hoppe and Russell* [1982] found that there is a linear relationship between the wave frequency and the magnetic field strength during various planetary encounters, indicating the wave frequencies depend on gyrofrequencies. The upstream wave frequencies at Mercury are the same as those of their counterparts at the Earth when scaled by the magnetic field strength [*Hoppe and Russell*, 1982; *Orlowski et al*., 1990]. Throughout this paper, we will use the term "30 second" waves to refer to the lower frequency (~ 5–10 s) waves at Mercury with properties similar to the 30 second waves at the Earth, and "1 Hz" waves to the higher frequency (~ 2 Hz) whistler waves at Mercury.

[5] The availability of MESSENGER orbiter data enables us to conduct an in-depth study of upstream waves in Mercury's foreshock. In this paper, we report the results of a preliminary survey of upstream waves at Mercury during a foreshock passage on 26 March 2011, using high-time resolution magnetic field data from the MESSENGER spacecraft. This preliminary study focuses on surveying the wave types, properties and their occurrence characteristics

2. Observations

2.1. Dataset and Bow Shock Model

[6] The MESSENGER magnetic field data are the only appropriate data set available for the study of upstream phenomena. *Anderson et al*. [2007] gives a detailed description of the magnetometer instrument. The plasma instrument onboard is not configured to measure the solar wind plasma and is not an appropriate instrument for characterizing the low-density backstreaming particles either. The MESSENGER calibrated fluxgate magnetometer data set archived in the Planetary Data System (PDS) has a resolution of 20 samples per second. To date, the Mercury flyby data plus orbital data from 23 March (day 82), 2011 to 17 May 2011 are available at PDS. Approximately 1300 of the ~1550 h of archived data is when the spacecraft was outside of Mercury's bow shock, either in the foreshock or undisturbed solar wind.

[7] MESSENGER is in an orbit of 80° inclination, with apohermion occurring in the southern hemisphere at 7.1 R_M (R_M is the radius of Mercury) and perihermion in the northern hemisphere at 1.1 R_M, and the orbital period is 12 h. During the period of the available data, the spacecraft apohermion moves from the midafternoon (~ 15 LT) toward dawn and into postmidnight sector, covering all the subsolar as well as the dawn flank upstream regions. Considering a small IMF cone angle (the angle between the IMF and the solar wind flow) or a nominal Parker spiral angle of ~ 20° (measuring from the Sun-Mercury line toward dawn) at Mercury, the MESSENGER spacecraft has a large probability of entering the foreshock region in every orbit. Thus, orbital coverage of the available MESSENGER data is ideally suited to address scientific questions in the foreshock.

[8] A bow shock model is required for a quantitative study of the upstream waves, such as determining the foreshock geometry, the location of the spacecraft relative to the bow shock, as well as the angle between the IMF and the bow shock normal θ_{Bn} [*Le and Russell*, 1992a]. We will use the empirical Mercury bow shock model of *Slavin et al*. [2009] in this study. *Slavin et al*. [2009], following *Slavin and Holzer* [1981], fitted the bow shock crossings of both the Mariner 10 and MESSENGER during Mercury flybys and determined the best fit bow shock model using a conic section whose focus is free to lie along the aberrated X axis

$$\sqrt{(X - X_0)^2 + Y^2 + Z^2} = \frac{L}{1 + \varepsilon \cdot \cos(\theta)}$$

where X_0 is the location of the focus, ε the eccentricity, L the semi-latus rectum, and the polar angle ε measured from the $+X$ axis about X_0. The fitting of shock crossings from both the Mariner 10 and MESSENGER flybys results in the fitting parameters: $X_0 = 0.5$ R_M, $\varepsilon = 1.07$, and $L = 2.40$ R_M (R_M is the Mercury radius). The subsolar standoff distance for this model is 1.66 R_M.

2.2. Overview of Observations

[9] Our preliminary observations clearly establish that the "1 Hz" whistler waves are the most abundant wave phenomenon in Mercury's foreshock. In the preliminary survey of the MESSENGER magnetic field data, we have observed evidence of upstream "1 Hz" whistler waves in every orbit of Mercury orbiting data we have surveyed. At Mercury,

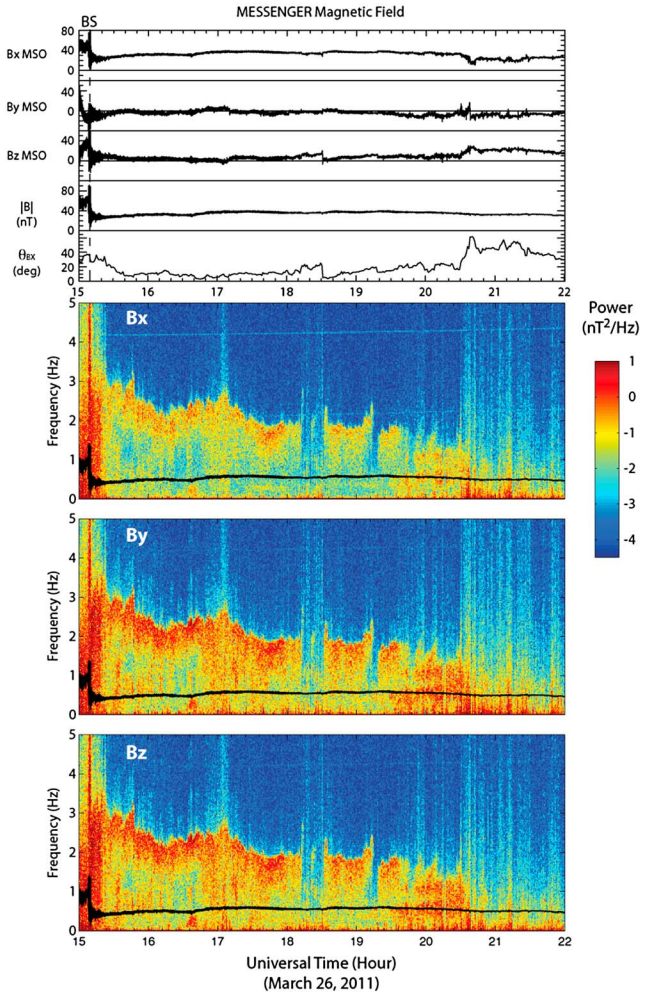

Figure 1. Overview of the MESSENGER magnetic field observations for the period from 15 to 22 UT on 26 March 2011. (top) The three components of the magnetic field vector (*Bx*, *By*, and *Bz*), the magnetic field strength (|*B*|), and the IMF cone angle (θ_{BX}, the angle between the IMF and the Mercury-Sun line). (bottom) The dynamic power spectrograms of the three components of the magnetic field. The black traces superposed on top of the power spectrogram represent the local proton gyrofrequency calculated from the background magnetic field strength.

the "1 Hz" whistler waves appear as long wave trains lasting for hours in the foreshock region.

[10] Figure 1 presents an overview of a good example demonstrating the occurrence characteristics of the long lasting "1 Hz" whistler waves on 26 March 2011. The top panel of Figure 1 displays 7 h of MESSENGER magnetic field data for the period from 15 to 22 UT on 26 March 2011, including the three components of the magnetic field vector (*Bx*, *By*, and *Bz*), the magnetic field strength (|*B*|), and the IMF cone angle (θ_{BX}). The magnetic field data are in their highest time resolution at 20 Hz sampling rate. They are in the Mercury solar orbital (MSO) coordinates, where $+X_{\mathrm{MSO}}$ points to the Sun from the planet's center, $+Y_{\mathrm{MSO}}$ is in the plane of Mercury's orbit and opposite to the planetary velocity vector, and $+Z_{\mathrm{MSO}}$ completes the right handed system. It is similar to the familiar Geocentric Solar Ecliptic coordinate system commonly used at the Earth. The IMF cone angle in Figure 1 is calculated using 60 s averaged magnetic field data. The bottom panels of Figure 1 show the dynamic power spectrograms of the three components of the magnetic field. The black traces superposed on top of the power spectrogram represent the local proton gyrofrequency calculated from the background magnetic field strength.

[11] Since the solar wind data for this pass are not available, the bow shock jump conditions and structures may shed some light on the solar wind Mach number. The bow shock crossing in Figure 1 occurs at ~ 15:10 UT as indicated by the dashed line in the top panel. Figure 2 displays a blow-up of the magnetic field data around this bow shock crossing showing the detailed shock jump condition. The top panel contains 4 min magnetic field data in MSO around the bow shock crossing. The bottom panel displays 1 min magnetic field data around the bow shock crossing in a shock normal coordinate system determined by the bow shock coplanarity analysis. In the shock normal coordinate system, *N* is the local bow shock normal direction, the *L*-*N* plane contains both the upstream and downstream magnetic field, and *M* is normal to both the upstream and downstream fields. For this bow shock crossing, the angle between the upstream magnetic field and the bow shock normal is 61° at the bow shock crossing. Whistler wave activities are apparent in the upstream magnetic field. The downstream magnetic field exhibits a very small overshoot. Comparing with the structures of the Earth's bow shocks at various Mach numbers in previous studies, the structure of this bow shock crossing resembles those of slightly subcritical or marginally critical shocks (the Mach number is slightly less or very close to the critical Mach number) [*Sckopke et al.*, 1990; *Farris et al.*, 1993]. Based on the bow shock structures, it is very likely that the solar wind Mach number is low for this pass.

[12] Figure 3 shows the MESSENGER spacecraft trajectory for the time interval in Figure 1. The top panel is the MESSENGER trajectory displayed in solar-wind-aberrated cylindrical MSO coordinates. The bottom panels are the projections of the same trajectory on the MSO *X*-*Y*, *X*-*Z*, and *Y*-*Z* planes, respectively. The empirical magnetopause and bow shock models based on Mariner 10 and MESSENGER data are also plotted in each panel [*Slavin et al.*, 2009]. In particular, the size of the bow shock is scaled to the actual bow shock crossing of MESSENGER at 15:10 UT.

[13] Immediately upstream from the bow shock (~ 15:10–15:20 UT), the upstream waves appear to be broad-band with high frequency cutoff at ~ 3.5 Hz as shown in Figure 1. Their irregular wave forms are shown in the upstream portion in Figure 2. After ~ 15:20 UT, the most striking feature in Figure 1 is the long-lasting narrow-band spectral power enhancement near 2 Hz. The bow shock crossing occurs at ~ 15:10 UT. The magnetic field fluctuations are very broadband up to ~ 3 Hz initially after the bow shock crossing. Starting ~ 15:20 UT, intense "1 Hz" whistler waves are present for more than 5 h, from ~ 15:10 UT to ~ 20:40 UT. Overall, we see a general decreasing trend of the "1 Hz" wave power as the spacecraft moves away from the bow shock. Meanwhile, the wave frequency exhibits a downward trend. The two short intervals at ~ 1810–1830 UT and

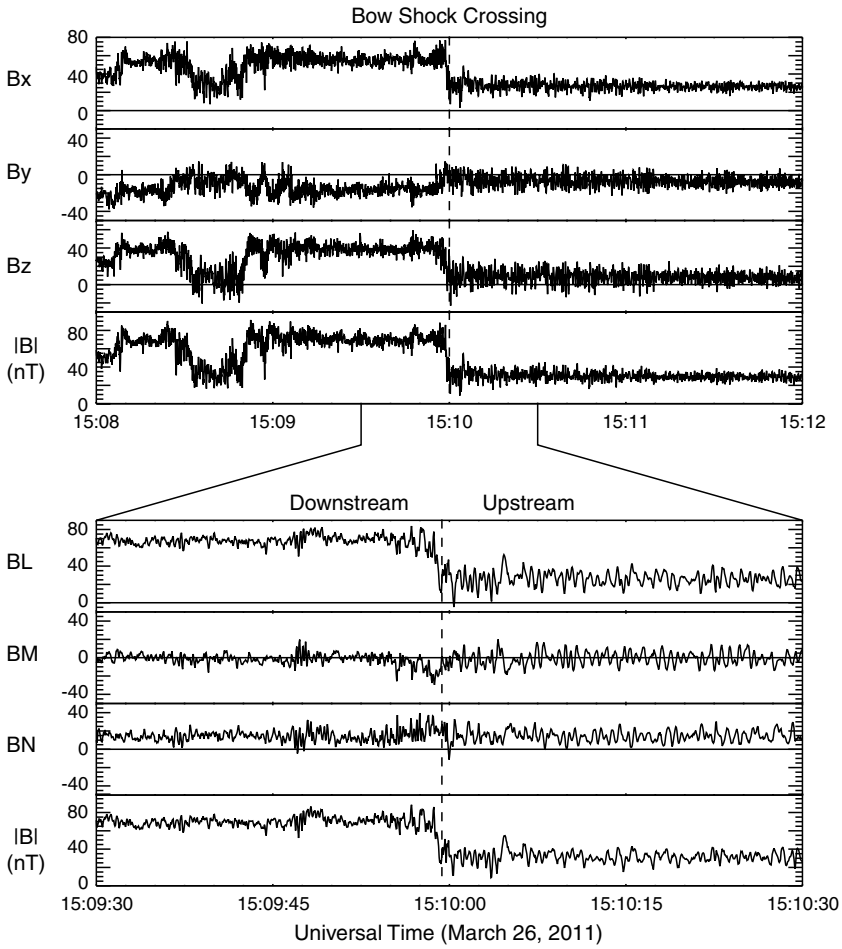

Figure 2. (top) 4 min magnetic field data in MSO around the bow shock crossing on 26 March 2011. (bottom) 1 min magnetic field data around the bow shock crossing in a shock normal coordinate system determined by the bow shock coplanarity analysis.

1914–1918 UT with greatly reduced or nearly diminished "1 Hz" wave power are apparently associated with changes of the IMF direction and we will discuss them further with regard to the foreshock geometry. In contrast to the Earth's foreshock where large-amplitude 30 second waves are the most common wave phenomenon, there is a general lack of "30 second" waves in Mercury's foreshock. In the bottom of Figure 1, it is evident that there are a few short intervals with enhanced lower frequency (less than 1 Hz) wave powers in the bottom panels of Figure 1. We will also discuss these intervals in more detail below.

[14] The changes of the IMF direction due to the increase of the IMF-*Bz* component at ~1810 UT and again at 1914 UT are apparently responsible for the reduced or nearly diminished "1 Hz" wave power in the two short intervals mentioned above. The IMF directional change at ~2040 UT also moves the spacecraft completely out of the foreshock region. The foreshock geometry can be simplified into a plane containing the velocity and the IMF (the so-called **V-B** plane) since the motion of upstream waves and particles is ordered by this plane [*Greenstadt and Baum*, 1986; *Le and Russell*, 1992a]. In this particular case, the **V-B** plane is roughly the MSO *XZ* plane as the IMF *By* component is nearly zero most of the time and always the smallest among the three components during the wave interval. Figure 4 displays the spacecraft trajectory in the aberrated *XZ* plane with the magnetopause and the bow shock scaled to MESSENGER's actual boundary crossings. The portions of the trajectory in red are the intervals with intense "1 Hz" whistler waves (except a brief interval ~ 1914–1918 UT) and in black without the intense waves.

[15] We show the foreshock geometry schematically for three IMF conditions in Figure 4. In Figure 4a, the IMF has a cone angle of 10°, corresponding to the average conditions in the intervals when MESSENGER observes intense "1 Hz" whistler waves (all the red segments of the orbit). The spacecraft is magnetically connected to the bow shock everywhere along the trajectory under this IMF condition. In Figure 4b, the IMF cone angle is increased to 20°, corresponding to the average condition in ~1810–1830 UT when the power of "1 Hz" is greatly reduced or diminished due to an increase in the IMF *Bz* component. Under this condition, the spacecraft is no longer connected to the bow shock in the later part of the trajectory, which includes the short black segment of the orbit. It explains why the "1 Hz" whistler waves are greatly reduced during ~1810–1830 UT. We will discuss why the "1 Hz" wave power is not completely absent under this condition. In Figure 4c, the IMF cone angle is further increased to 45°, corresponding to the condition after 2040 UT due to the much-enhanced IMF *Bz* magnitude,

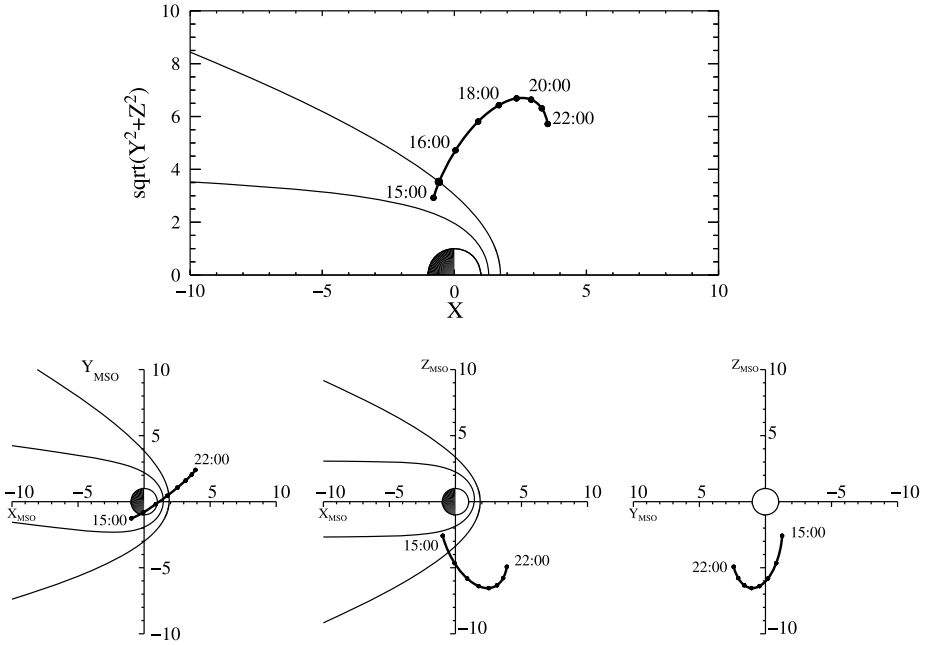

Figure 3. The MESSENGER spacecraft trajectory for the time interval in Figure 1. (top) The MESSENGER trajectory in solar-wind-aberrated cylindrical MSO coordinates. (bottom) The projections of the trajectory on the MSO *X-Y*, *X-Z*, and *Y-Z* planes, respectively. The empirical magnetopause and bow shock models based on Mariner 10 and MESSENGER data are plotted in each panel.

which becomes comparable to the *Bx* magnitude. Under this condition, the spacecraft moves out of the foreshock and is no longer connected to the bow shock, resulting in the cutoff of the waves. Figure 4 demonstrates that intense "1 Hz" whistler waves have been observed everywhere when the spacecraft is in the foreshock and magnetically connected to the bow shock during this pass. This is consistent to the propagation of whistler waves with source point at the bow shock since theory shows that their group velocity is approximately guided by the magnetic field [*Swanson*, 2003].

2.3. Observations of "1 Hz" Whistler Waves

2.3.1. Properties of "1 Hz" Whistler Waves

[16] The properties of the upstream "1 Hz" whistler waves at Mercury appear to be similar to those reported at the Earth. Figure 5 presents an example of the "1 Hz" whistler waves and the wave properties. Figure 5a contains 5 min of the highest resolution magnetic field from MESSENGER in MSO coordinates, representative of the "1 Hz" whistler waves for the entire pass. Figure 5b is an expanded view of the 30 s data within the two dashed lines in Figure 5a, showing the detailed waveform and its nearly monochromatic nature.

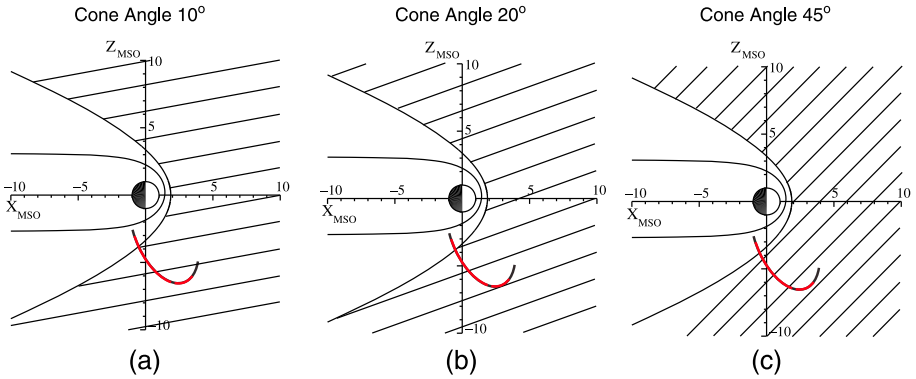

Figure 4. The spacecraft trajectory and the foreshock geometry schematics in aberrated MSO *XZ* plane for three IMF cone angles: (a) 10°, (b) 20°, and (c) 45°. The magnetopause and the bow shock are scaled to MESSENGER's actual boundary crossings. The portions of the trajectory in red are the intervals with intense "1 Hz" whistler waves (except a brief interval ~ 1914–1918 UT) and in black without the intense waves.

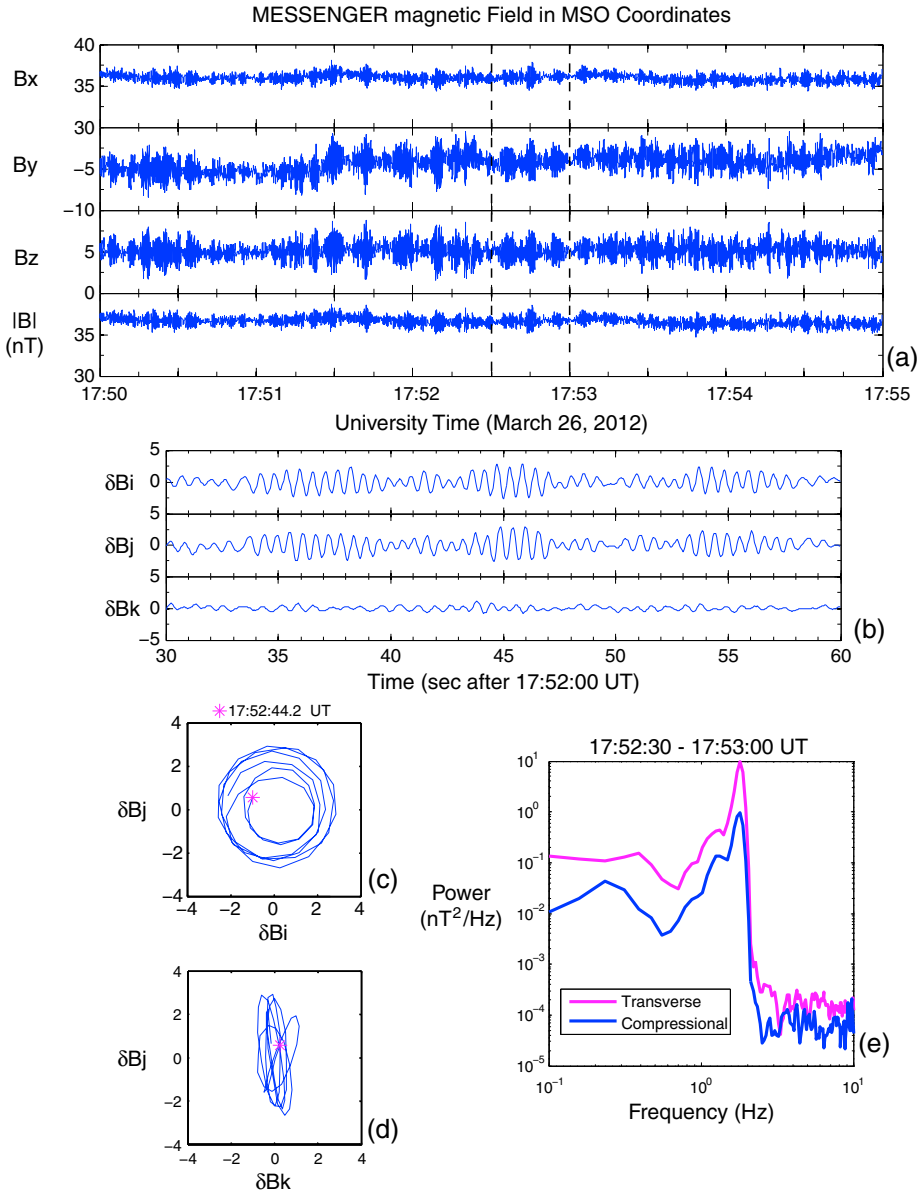

Figure 5. An example of the "1 Hz" whistler waves at Mercury. (a) Time series of 5 min high-resolution MESSENGER magnetic field data in MSO coordinates; (b) expanded view of the 30 s data within the two dashed lines in Figure 5a, displayed in the coordinate system determined by the minimum variance analysis (MVA); (c and d) hodograms for 6 cycles of the wave magnetic field starting from 17:52:44.2 UT; and (e) transverse and compressional power spectra for the "1 Hz" whistler waves in Figure 5b.

The data in Figure 5b are displayed in the coordinate system determined by the minimum variance analysis (MVA) [*Sonnerup and Cahill*, 1967], where **i**, **j**, and **k** correspond to the directions of the maximum, intermediate, and minimum variances, respectively, and **k** is also the wave vector direction (with 180° ambiguity). The minimum variance analysis shows that the wave propagates obliquely to the background magnetic field, as the angle between **k** and the average magnetic field **B** is 22.8°. This moderate propagating angle is consistent with the wave being moderately compressional as evident by the small wave amplitude in the δB_k component. The waves are left-handed polarized in the spacecraft frame with an ellipticity of −0.88. The polarization properties are also evident in Figures 4c and 4d, showing the hodograms for 6 cycles of the wave magnetic field starting from 17:52:44.2 UT. Figure 5e shows the transverse and compressional power spectra for the "1 Hz" whistler waves in Figure 5b. The spectral peak is at ~ 1.8 Hz and narrow-banded with a sharp cutoff at the high frequency edge at ~ 2 Hz. The sharp high-frequency cutoff edge is also evident in the dynamic power spectrogram in Figure 1.

[17] The wave properties presented above are common for all the "1 Hz" whistler waves observed in the entire pass. Figure 6 shows the wave properties as a function of time during the entire wave interval. The top three panels are the frequency-time spectrograms of the wave ellipticity (Figure 6a), the propagation angle between the wave normal

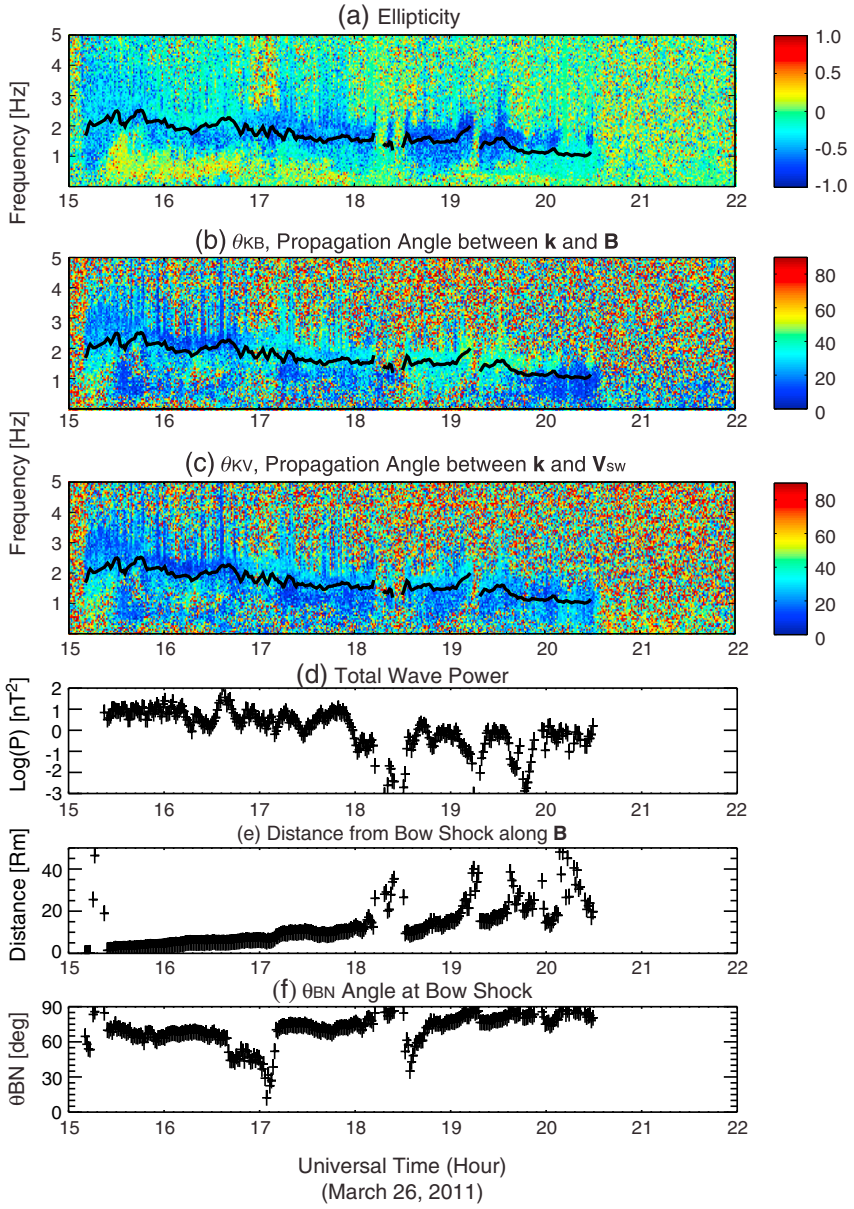

Figure 6. Properties of the "1 Hz" whistler waves as a function of time during the entire wave interval: (a) the frequency-time spectrograms of the wave ellipticity; (b) the propagation angle between the wave normal and the magnetic field θ_{kB}; (c) the propagation angle between the wave normal and the solar wind flow θ_{kV}; (d) the total wave power integrated in the 0.8–3.3 Hz frequency band; (e) the distance from the bow shock along the magnetic field; and (f) the angle between the magnetic field and the bow shock normal direction at the source point θ_{BN}.

and the magnetic field θ_{kB} (Figure 6b), and the propagation angle between the wave normal and the solar wind flow θ_{kV} (Figure 6c). The black traces are the wave frequency for the "1 Hz" whistler waves, calculated as the weighted frequency in the frequency band of 0.8–3.3 Hz. The wave propagation angle θ_{kB} for the "1 Hz" waves occurs in the range from 20° to 40° after the bow shock crossing until ~19:40 UT. The wave polarization is consistently left-handed with the ellipticity ~ −0.8 in the spacecraft frame. After ~19:40 UT, apparently associated with the IMF By turning more negative, the wave propagation becomes more parallel to the magnetic field as the propagation angle θ_{kB} decreases to ~10° and less, and the polarization remains left-handed. The propagation angle from the aberrated solar wind flow direction θ_{kV} determines the effect of Doppler shifting by the solar wind flow. The smaller the angle θ_{kV} is, the greater Doppler shifting the wave frequency has. Figure 6c shows that this angle is very small, less than ~20°. Thus, Doppler shifting of the frequency is expected to be significant. The "1 Hz" whistler waves are intrinsically right-handed polarized in the plasma rest frame. They can propagate upstream because their group velocity is generally greater than the solar wind velocity [*Orlowski and Russell*, 1991]. However, their phase velocity is smaller than the solar wind velocity, and thus, their polarization as observed by the spacecraft is reversed to left-handed due to the Doppler shift effect.

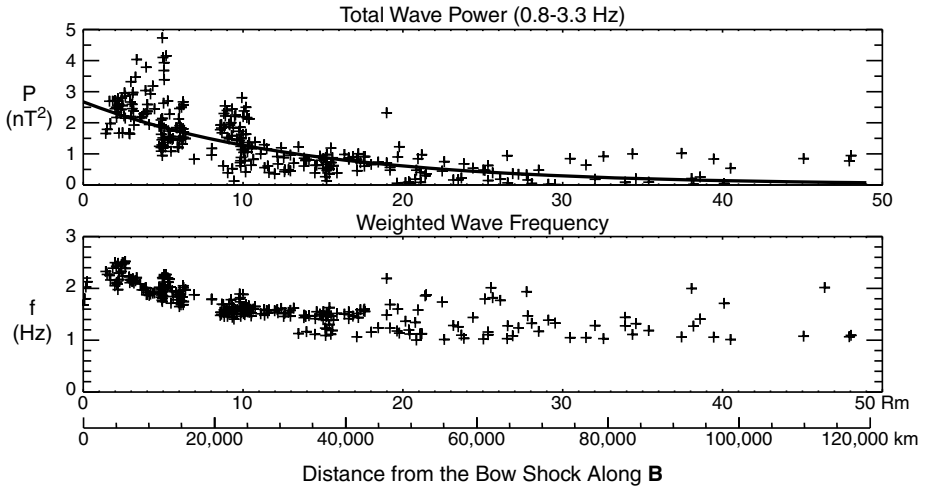

Figure 7. (top) The total power and (bottom) the weighted frequency of the "1 Hz" whistler waves as a function of the distance from the bow shock along the magnetic field line.

[18] Figure 6d shows the total wave power integrated in the same 0.8–3.3 Hz frequency band. The wave power is quite variable with a general decreasing trend as the spacecraft moves away from the bow shock. Figure 6e shows the distance between the spacecraft and the source point at the model bow shock at the 1 min cadence. The source point is where the magnetic field line from the spacecraft intersects the bow shock. It is calculated using the instantaneous 1 min average of the magnetic field vector. For the times when the spacecraft is not magnetically connected to the bow shock, or when the distance is greater than 50 R_M (the Mercury radius), no data points are plotted in Figure 6c. Figure 6f shows the θ_{BN}, the angle between the magnetic field and the bow shock normal direction at the source point. It indicates whether the spacecraft is connected to the quasi-perpendicular ($\theta_{BN} > \sim 45°$) or the quasi-parallel ($\theta_{BN} < \sim 45°$) portion of the bow shock. It shows that the spacecraft is connected to the quasi-perpendicular portion of the bow shock most of the time except two brief periods around ~1705 UT and ~1835 UT. Nevertheless, the range of θ_{BN} variation is large enough to examine if there is any correlations between the wave properties and the θ_{BN} angle at the bow shock source point. It shows there is no clear correlation between the wave properties and the θ_{BN} angle at the source point.

[19] Although the spacecraft distance from the bow shock increases monotonically as the spacecraft moves away from the bow shock in this particular pass, the distance from the bow shock along the magnetic field line does not. The source point on the bow shock moves back and forth due to the variability of the magnetic field direction, and the distance between the spacecraft and the source point varies accordingly. From Figure 6, it appears that the total wave power and the weighted wave frequency have better correlations with the distance from the spacecraft to the bow shock along the magnetic field. In Figure 7, we display the total power (top) and the weighted frequency (bottom) of the "1 Hz" whistler waves as a function of the distance from the bow shock along the magnetic field line. The solid line in the top panel is the result of the least squares fitting of the wave power P using an exponential function of distance L

$$P = P_o \cdot \exp(-L/L_o)$$

[20] The least squares fitting results give that (1) the wave power (amplitude) at the bow shock, P_o, is ~2.7 nT^2 (~ 1.6 nT); and (2) the scale length of the wave power falloff , L_o, is ~ 13.5 R_M, or ~33,000 km. In the bottom panel, there is also a clear decreasing trend of weighted wave frequency as the distance from the spacecraft and the source point on the bow shock increases. Assuming that the wave power generated at the bow shock is independent of wave frequency, it shows lower frequency waves can reach farther upstream from the bow shocks.

2.3.2. Remnant "1 Hz" Waves on Unconnected Field Lines

[21] We have observed that the "1 Hz" wave power is greatly reduced or diminished during the periods when the IMF changes its direction toward a larger IMF cone angle (Figure 1). The larger IMF cone angles result in the spacecraft increasing the distance from the bow shock along **B** or even not being connected to the bow shock magnetically. A close examination of the data near the time of IMF changing directions reveals that the "1 Hz" wave power does not turn off immediately after the IMF changes direction. The waves can still be present for a couple of minutes on field-lines that are clearly no longer connected to the bow shock magnetically. They disappear gradually after the spacecraft switches from connected to unconnected condition. Figure 8 presents one of such cases. The top panel of Figure 8 shows the dynamic power spectrum for 30 min of data from 18:05–18:35 UT. The change of the IMF direction occurs around 18:12:10 UT, marked by a white dashed line in the top panel. The middle panel shows the detailed magnetic field data around the time when the IMF changed its direction. The bottom panels show the foreshock geometry with the spacecraft location before and after the IMF directional change, corresponding to 1 min intervals (Figures 8a and 8b), respectively. In the foreshock geometry plot, the vector denoted by **B** is the IMF direction, determined by the 1 min magnetic field average. The vector denoted by $\mathbf{V}_{sw}$ is the aberrated solar wind flow direction. The two vectors $\mathbf{V}_{sw}$ and **B** define the **V-B** plane, and the bow shock is the cross-section of the 3-D model bow shock on the **V-B** plane.

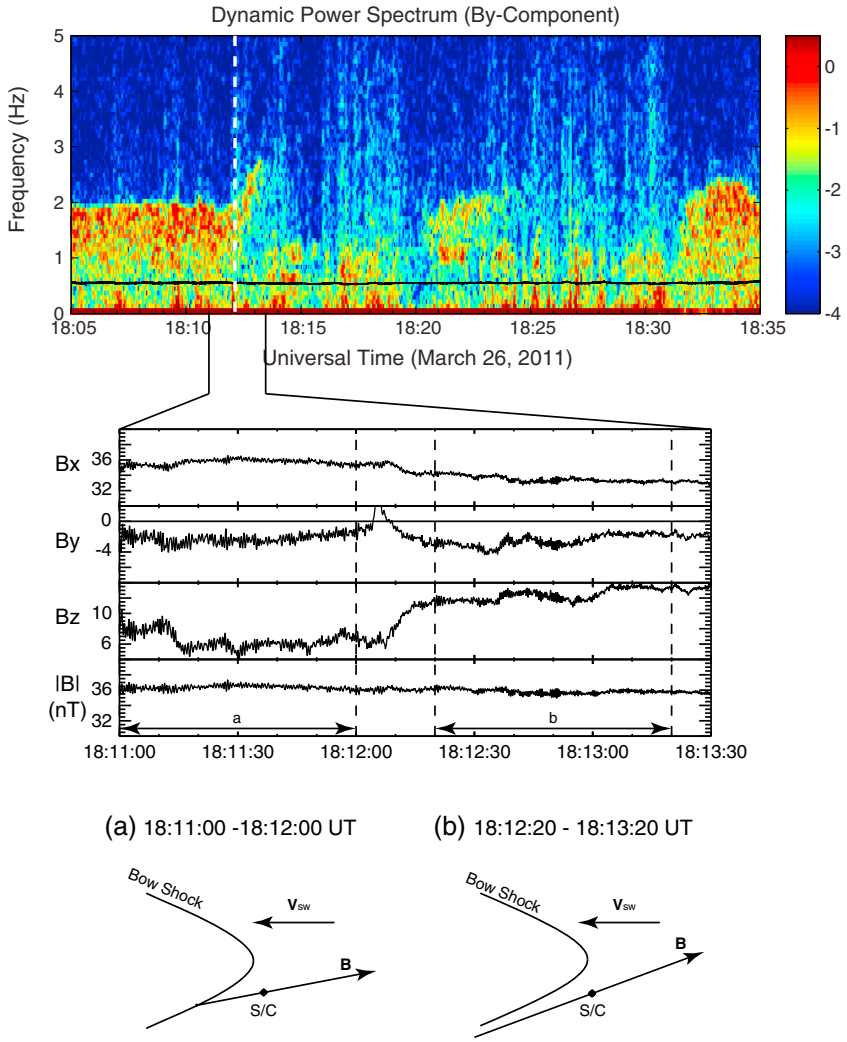

Figure 8. (top) The dynamic power spectrum for 30 min of data from 18:05–18:35 UT. The change of the IMF direction occurs around 18:12:10 UT, marked by a white dashed line in the top panel. (middle) Detailed magnetic field data around the IMF changing direction. (bottom) The foreshock geometry before and after the IMF changing direction.

The model bow shock is scaled by the spacecraft location at the actual bow shock crossing at 15:10 UT. The dot denoted by S/C is the spacecraft position. Immediately before the magnetic field directional change, the IMF cone angle is 11°, and the spacecraft is connected to the quasi-perpendicular bow shock with a distance of 12.5 R_M. After the IMF cone angle increases to 20°, the spacecraft becomes unconnected to the bow shock. Both the dynamic power spectrum and the magnetic field data show that the "1 Hz" waves remain to be present for about 1 min after the cone angle increase. However, the wave frequency exhibits an increasing trend in this case. The amplitude of the remnant waves gradually decreases to zero. The polarization of the remnant waves remains left-handed (Figure 6).

2.4. Observations of Lower Frequency Waves

[22] In the Earth's foreshock, lower frequency waves (commonly referred as the 30 second waves) are an intrinsic feature observed in the ion foreshock, the region connected mostly to the quasi-parallel bow shock with θ_{BN} generally less than ~ 50° [*Le and Russell*, 1992a]. These waves are generated by ions streaming upstream along the magnetic field lines from the bow shock via the resonant instability between the right-handed magnetosonic waves and the backstreaming ions. They appear with different waveforms depending on the location: nearly sinusoidal waves near the ion foreshock boundary, compressional waves with steepening edges deep into the foreshock, and very irregular nonlinear waves near the bow shock [*Hoppe et al*., 1982; *Le and Russell*, 1992a, 1992b]. Most of the time they are very strong with amplitudes in the same order of the background field strength. They are present all the time when the spacecraft is in the ion foreshock. In the 26 March 2011 pass, there are two short intervals when θ_{BN} is less than 50°, ~ 16:40–17:10 UT and ~ 18:34–18:37 UT (ref. Figure 6). Unlike the observations in the Earth's foreshock, we do not see a persistent narrow-band power enhancement at lower frequency band in the quasi-parallel foreshock of Mercury, as evident in the dynamic power spectra in Figure 1. It appears that low frequency waves

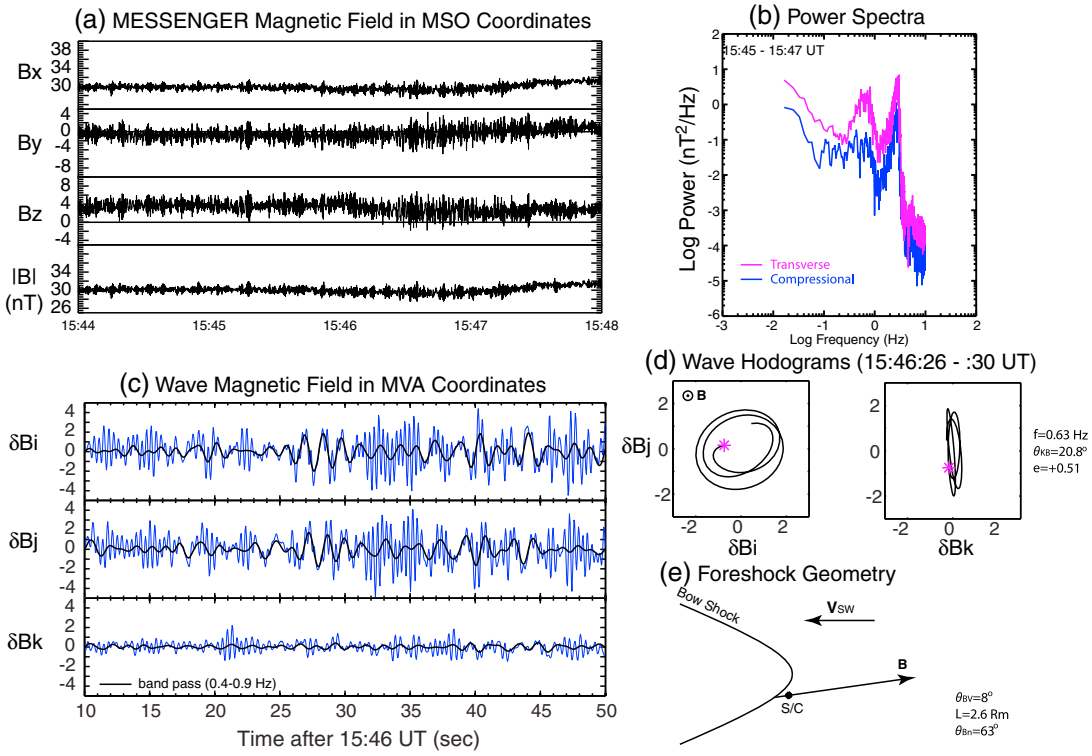

Figure 9. An example of the lower frequency bursts at ~ 0.8 Hz: (a) the MESSENGER magnetic field data in MSO; (b) the transverse and compressional power spectra; (c) a 40 s interval for the detrended ion data (blue) and the low-pass filtered data (black) in MVA coordinates; (d) the hodograms of the waves in MVA; and (e) the corresponding foreshock geometry.

occur sporadically with short durations. We can identify a few short bursts of spectral power enhancement with frequencies below those of "1 Hz" waves, both in the quasi-perpendicular and quasi-parallel foreshocks. The observations of the lower frequency waves involve two frequency bands: ~ 0.8 Hz and ~ 0.3 Hz waves, respectively. Herein we present examples and the analysis of these lower frequency waves.

2.4.1. Waves at ~ 0.8 Hz

[23] Figure 9 shows one example of the lower frequency bursts at ~ 0.8 Hz. Figure 9a contains 4 min of the MESSENGER magnetic field data in MSO, and Figure 9b power spectra for 2 min of the data. Two distinct spectral peaks are evident in Figure 9b. Besides the peak at ~ 3 Hz, which is the "1 Hz" whistler waves we have discussed above, there is another spectral peak at lower frequency ~ 0.8 Hz. Because these lower frequency waves coexist with the intense "1 Hz" waves, it is difficult to discern their waveforms in the highest time resolution data in Figure 9a. To examine these lower frequency waves, we display a 40 s interval for both the detrended high-resolution data (blue) as well as the low-pass filtered data (black) in Figure 9c. These data are rotated to the coordinated system determined by the MVA, where **i**, **j**, and **k** correspond to the directions of the maximum, intermediate, and minimum variances, respectively, and **k** is also the wave vector direction (with 180° ambiguity). The lower frequency waves have peak-to-peak amplitudes ~ 1–4 nT, lower than those of "1 Hz" whistler waves. Wave analysis results show that the lower frequency waves are right-handed polarized in the spacecraft frame, which is in the opposite sense to the "1 Hz" whistler waves. Figure 9e shows the corresponding foreshock geometry for the time interval. The aberrated IMF cone angle (θ_{BV}) is 8°. The spacecraft is ~ 2.6 R_M from the bow shock along the magnetic field line. The angle between the magnetic field and the bow shock normal (θ_{Bn}) at the source point is 63°. Thus the spacecraft is connected to the quasi-perpendicular shock.

[24] This type of the waves has not been reported previously at Mercury in Mariner 10 data.

2.4.2. Waves at ~ 0.3 Hz (the "30 second" Fast Magnetosonic Waves at Mercury)

[25] In the power spectrograms in Figure 1, a short burst of enhanced power at ~ 0.3 Hz near ~ 16:30 UT is clearly visible. There are also a few weaker bursts within 17–18 UT. Figure 10 shows an example of the waves for the lower frequency burst at ~ 0.3 Hz. It is in the same format as in Figure 9. In this case, the power spectra exhibit three distinct peaks: the two arrows in Figure 10b indicate the two lower frequency peaks in addition to the "1 Hz" whistler waves. The middle peak occurs at ~ 1 Hz and the wave analysis shows that the waves at this frequency appear to be the same type as the 0.8 Hz lower frequency waves in Figure 9 since these waves have similar properties (frequency, propagation angle, polarization, and ellipticity). Here we only focus on the detailed wave analysis for the spectral peak at ~ 0.3 Hz in Figures 10c and 10d using low-pass filtered data with a 0.6 Hz cut off frequency. Figure 10e shows the corresponding foreshock geometry for the time interval. This is a case with nearly radial IMF as the aberrated IMF cone angle (θ_{BV}) is very small at 3°. The spacecraft is ~ 5.1

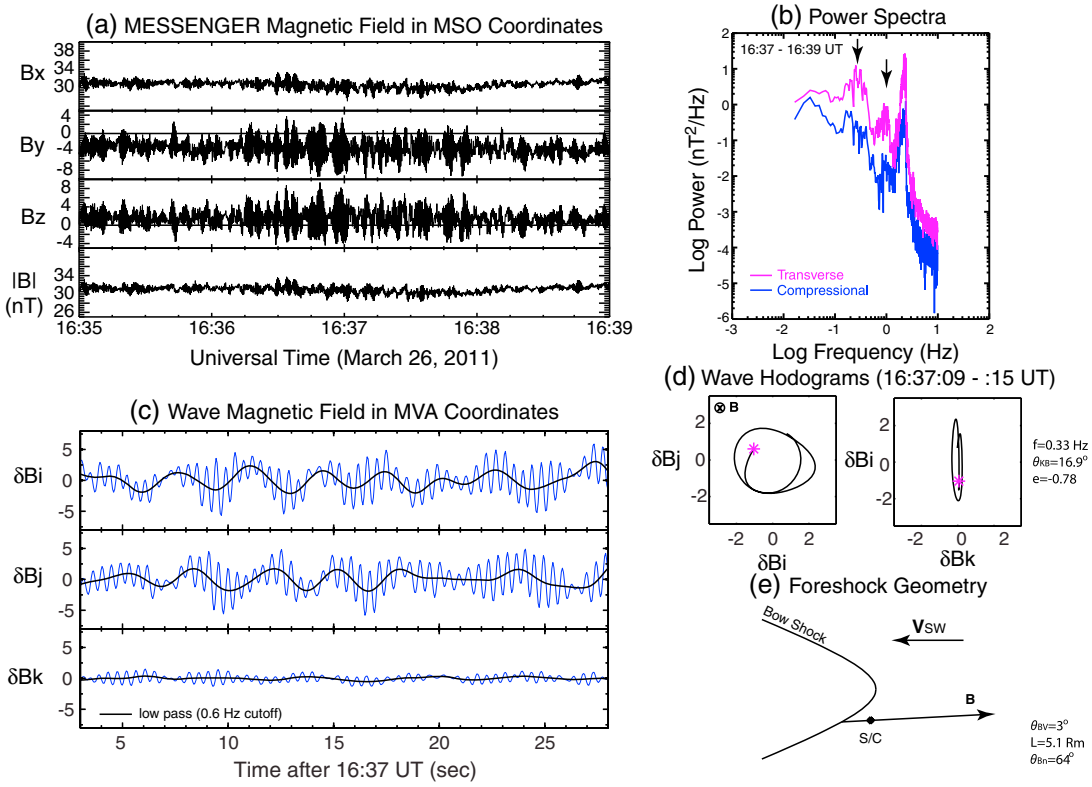

Figure 10. An example of the lower frequency bursts at ~0.3 Hz in the same format as in Figure 9.

R_M from the bow shock along the magnetic field line. The angle between the magnetic field and the bow shock normal (θ_{Bn}) at the source point is 64°.

[26] The waves at ~0.3 Hz appear to be left-handed polarized in the spacecraft frame. The peak-to-peak wave amplitudes are ~3 nT, which is in the order of 10% of the background magnetic field strength. The frequency and the polarization both agree with the properties of 30 second waves. Previous observations have established that the frequency of 30 second waves in the spacecraft frame depends mainly on the magnetic field strength [*Hoppe and Russell*, 1982; *Le and Russell*, 1996]. Based on the empirical scaling relation, the frequency of the "30 second" waves in Mercury's foreshock would be ~0.2–0.3 Hz for the IMF strength 30–50 nT.

3. Discussions

[27] Previous studies of planetary upstream waves have demonstrated that categorizing the waves based on their frequency is an appropriate approach. Based on the wave properties and their frequency characteristics, upstream waves have been classified into different types based on the frequency ranges in the spacecraft frame. Our detailed examination of the MESSENGER magnetic field data reveals the following occurrence characteristics of Mercury upstream waves:

[28] 1. The "1 Hz" whistler waves with frequencies ~2 Hz appear to be the most abundant wave phenomenon in Mercury's foreshock. They appear as long wave trains and sometimes last for hours in the foreshock. Their wave properties are very similar to those at the Earth.

[29] 2. The "30 second" magnetosonic waves generated by backstreaming ions correspond to the spectral peak at the lowest frequency at ~0.3 Hz. The "30 second" waves occur sporadically in Mercury's foreshock. They appear to be very similar to the 30 second sinusoidal waves near the Earth's ion foreshock boundary, but with much smaller amplitudes. We have not observed the "30 second" waves with steepening edges, i.e., in the form of shocklets, in our preliminary survey.

[30] 3. Short bursts of spectral peaks at ~0.8 Hz are also observed in Mercury's foreshock. This is a new observation at Mercury. Waves at this frequency were not reported previously in Mariner 10 data. It is not clear if they are similar to the 3 second waves at the Earth. So far, we only see these waves coexisting with the "1 Hz" whistler waves and/or "30 second" magnetosonic waves.

[31] Despite the similar wave properties at Mercury and the Earth, both Mariner 10 and MESSENGER data show that the wave occurrence characteristics at Mercury and Earth are quite different. The most striking difference lies on the occurrence characteristics of lower frequency "30 second" magnetosonic waves at Mercury. The large-amplitude 30 second magnetosonic waves at the Earth are found to be an intrinsic feature in the Earth's foreshock (see *Eastwood et al.* [2005] for a review). They appear whenever the spacecraft is upstream from the quasi-parallel shock. They often have very distinct waveforms, as nearly sinusoidal waves near the ion foreshock boundary, or as shocklets with steepened leading edges deep into the foreshock region [*Greenstadt et al.*, 1968; *Hoppe et al.*, 1981, 1982]. The waves have smaller amplitudes and propagate nearly parallel to the magnetic field when in the nearly sinusoidal form. However, the waves typically grow to very large amplitudes

($\delta B/B \sim 100\%$), and they propagate obliquely to the magnetic field when in the steepened waveform, which is attributed to the result of nonlinear evolution [e.g., *Omidi and Winske*, 1990]. In contrast, the "30 second" magnetosonic waves are present only sporadically in Mercury's foreshock. Their wave amplitudes are generally small ($\delta B/B \sim 10\%$) in our limited observations. Neither Mariner 10 nor MESSENGER has observed these waves in the steepening waveform, common to the upstream waves in the Earth's foreshock, and this observation is consistent with the observed small wave amplitudes and small wave propagation angles.

[32] Since backstreaming ions in the foreshock provide the free energy source for the "30 second" magnetosonic waves, the weak magnetosonic waves and the lack of shocklets (those in steepened waveforms) at Mercury imply that the backstreaming ion beams are much weaker in Mercury's foreshock than in the Earth's foreshock. The main reason is the low Mach number solar wind condition at Mercury (Figure 2). It has long been known that ion reflection is a general characteristic of high Mach number collisionless shocks [*Biskamp*, 1973; *Sonnerup*, 1969; *Paschmann et al*., 1980]. Theoretically, there is a critical Mach number, below which resistivity alone can account for all the dissipation to sustain the steady state shock transition, but above which other mechanisms such as ion reflections must be introduced to provide the necessary dissipation (see *Kennel et al*. [1985] and *Burgess et al*. [2012] for reviews). Observations at the Earth's bow shock show that a significant amount of solar wind ions, up to ~20%, would be reflected from the bow shock for conditions above the critical Alfvénic Mach number ($M_A > 2.5$–3); the reflected ions can escape the bow shock to form strong backstreaming ion beams in the incoming solar wind upstream from the quasi-parallel bow shock (see *Gosling and Robson* [1985] for a review). At low Mach numbers ($M_A \sim 2.0$–3.7), the ion reflections are observed to be at a lower level, which contribute to the modest level of upstream waves activities [*Thomsen et al*., 1985, 1993; *Sckopke et al*., 1990]. The solar wind Alfvénic Mach numbers at Mercury are expected to be in the range of ~4 to 6, which are generally right at or just above the critical Alfvénic Mach number. For the case presented in this paper, the magnetic structures of the bow shock crossing imply a slightly subcritical or marginally critical bow shock. This is in agreement with the lack of strong backstreaming beams. Although the leakage of downstream heated ions has also been considered as a source of upstream beams [*Edmiston et al*., 1982; *Tanaka et al*., 1983], observations show that this mechanism does not appear to be important for a low Mach number bow shock [*Kucharek et al*., 2004]. The upstream waves presented in this paper were observed mainly in the region off the subsolar foreshock. It is of great interest to examine the wave characteristics in the region upstream from subsolar bow shock. If the whistler waves were indeed dominant everywhere in Mercury's foreshock region, it would imply a very different interaction between the bow shock and foreshock at the Earth and Mercury. At the bow shock transition, upstream particles convey the bulk of the energy to the upstream region at the Earth whereas the upstream whistler waves play the similar role at Mercury. We will address this in the follow-up study.

[33] Another reason for the weak magnetosonic waves and the lack of shocklets in Mercury' foreshock is likely to be the fact that the small sizes of Mercury's magnetosphere and bow shock only support weak wave growth. The standoff distance of Mercury's magnetopause is only about 1/20 of the Earth's magnetopause [*Russell*, 1994]. Since the foreshock interaction region is where the IMF is connected to the bow shock, the time of connection for a field line to the bow shock is significantly smaller at Mercury than at the Earth as the field line moves with the solar wind passing the planet. Upstream magnetosonic waves are generated within the foreshock region by backstreaming ions, and grow in a parcel of solar wind plasma as they are carried downstream by the solar wind. The short connection time also means short growth time for the waves. Thus, the small bow shock size also works against the growth of the upstream magnetosonic waves. Furthermore, global hybrid simulations show that the nearly sinusoidal magnetosonic waves and the steepened magnetosonic waves (shocklets) are generated separately by different types of backstreaming ions in different regions of the foreshock, and their generations also depend on the magnetospheric scale sizes [*Omidi et al*., 2005; *Blanco-Cano et al*., 2006]. In their simulations of the solar wind interaction with small magnetospheres, *Blanco-Cano et al*. [2006] find that nearly sinusoidal parallel propagating waves are generated by field-aligned backstreaming beams. These waves are largely transverse and do not steepen. The steepened waveform is a result of nonlinear evolution of obliquely propagating magnetosonic waves (that are highly compressional). The compressional waves are generated by gyrating ion beams upstream from the quasi-parallel shocks when the magnetospheric/bow shock scale sizes are much larger.

[34] The upstream region of interplanetary shocks provides us another opportunity to study upstream waves in front of shocks for varying Mach numbers. Low Mach number condition occurs rarely at the Earth's bow shock, but frequently in interplanetary space [*Russell et al*., 2009]. Low-frequency magnetosonic waves similar to the 30 second waves at Earth have been observed upstream from both high and low Mach number interplanetary shocks [*Wilson et al*., 2009; *Kajdic et al*., 2012]. However, steepened waveforms, or shocklets, have only been reported upstream from a few interplanetary shocks with higher magnetosonic Mach numbers, ~ 3 in *Lucek and Balogh* [1997] and ~4 in *Wilson et al*. [2009]. In the survey of STEREO interplanetary shocks with low magnetosonic Mach numbers (≤ 2.3) presented in *Blanco-Cano et al*. [2013], no steepened waveforms and therefore no shocklets have been observed in the upstream region.

[35] Now we return to the occurrence characteristics of the "1 Hz" whistler waves. The "1 Hz" whistler waves appear to be the most common upstream waves at Mercury. Mariner 10 observed them in all the flyby encounters, both inbound and outbound [*Fairfield and Behannon*, 1976; *Orlowski et al*., 1990]. In our visual inspection of available MESSENGER data, their occurrence is also very common in the foreshock region. In the MESSENGER data we analyze in this paper, the waves are present for the entire period when the IMF is connected to the bow shock. Mercury "1 Hz" waves appear to be wave packets in long wave trains persisting throughout the foreshock region at

Mercury. They are present in the region upstream from both the quasi-parallel and the quasi-perpendicular shock. Their amplitudes are up to ~ 5 nT peak-to-peak, generally stronger than those of the 1 Hz waves at the Earth (~ 1 nT). However, the normalized wave amplitudes ($\delta B/B$) are similar at the two planets since the IMF strength is greater at Mercury than at the Earth. In the Earth's foreshock, the 1 Hz whistler waves are seen mainly in the region close to the bow shock and upstream from quasi-perpendicular shock. They do not go far upstream from the bow shock as the 30 second magnetosonic waves do. However, we believe that the apparent occurrence difference is mainly due to the difference sizes of the bow shocks at the two planets. The occurrence characteristics of the "1 Hz" whistler waves are essentially the same at the two planets. Unlike the "30 second" magnetosonic waves that are generated in the upstream region, the "1 Hz" whistler waves are generated at the bow shock. *Fairfield* [1974] first identified these waves as oblique whistlers and proposed the shock generation mechanisms for these waves. Subsequent comparative studies at planetary foreshocks support this mechanism [*Orlowski et al*., 1990, 1993, 1995; *Russell*, 2007]. The main evidence lies in the observations that the waves damp with the distance from the bow shock along the magnetic field line [*Orlowski and Russell*, 1991; *Orlowski et al*., 1995]. The more interesting observation is that there is a single damping scale length for the wave amplitudes observed at different planets, which is in the order of ~ 30,000 km [*Russell*, 2007]. This scale length translates to ~ 5 R_E, or ~ 15 R_M. Our observations at Mercury once again result in the same damping scale length (see Figure 7). This same scale length, ~ 15 R_M or ~ 5 R_E, accounts for the major part of the foreshock region at Mercury, but only a small fraction of the Earth's foreshock region. Although the "1 Hz" waves at Mercury have larger amplitudes, their wave properties are very similar to those in the Earth's foreshock. These observations imply that the wave generation is generic to the bow shock. The generation of the whistler waves is not affected by the strength and size of the bow shock in this parameter regime. Since the wave amplitudes are larger at Mercury than at the Earth, the lower Mach number conditions appear to be more favorable for the wave generation. This is also consistent to the larger background magnetic field strength at Mercury.

[36] In the upstream region, the whistler waves are the only mode of electromagnetic waves that can propagate upstream against the incoming solar wind flow. Their group velocity can reach three times the value of the phase velocity [*Russell*, 2007] and allows Poynting flux of the waves to be directed upstream [*Sundkvist et al*., 2012]. In this study, the observed wave remnants on newly disconnected magnetic field lines (see Figure 8) support the hypothesis that whistler wave packets move upstream against the solar wind. After leaving the bow shock and propagating upstream, the whistler waves are subject to strong Landau damping, which has been proposed to be the main cause of the observed amplitude falloff with the distance from the bow shock. The main evidence supporting this damping mechanism is the observation that the waves damp more strongly when propagating at greater angles to the magnetic field, as predicted by Landau resonance theory [*Russell*, 2007]. In this study, we present a long interval of the "1 Hz" whistler waves. The wave propagating angle relative to the magnetic field remains in the range of 20°–40° for almost the entire interval (Figure 6). Only in the last 30 min or so, the wave propagating angle drops to ~ 10°. We observe similar wave damping with the distance from the bow shock in this study. Although this is not inconsistent with the Landau damping prediction, our observations provide more insight to the wave damping. Associated with wave damping, we also observe a decreasing trend of the wave frequency (Figure 7). It implies the lower-frequency waves damp more slowly, and can propagate further upstream than the high-frequency waves.

[37] The occurrence characteristics of the "30 second" magnetosonic waves and "1 Hz" whistler waves in Mercury's foreshock also have implications to the low-frequency waves in the magnetosheath. The magnetosheath contains the shocked solar wind plasma and is known to have a boardband turbulent spectrum (see *Schwartz et al*. [1996] for a review). Often the magnetic fluctuations are a mixture of wave modes from different sources. Some waves are generated by local plasma instabilities related to the magnetopause or bow shock; some are carried through from the upstream region. Since the "1 Hz" whistler waves propagate upstream from the bow shock, they do not enter the magnetosheath and the magnetosphere. Thus, the "1 Hz" whistler waves do not contribute to the turbulent spectra in the magnetosheath and magnetosphere and are not responsible for the waves in the same frequency ranges within these two regions as well as on the ground. On the other hand, the "30 second" magnetosonic waves cannot propagate upstream and are convected downstream into the magnetosheath. In the Earth's magnetosheath, they are a major source of low-frequency magnetic turbulence downstream from the quasi-parallel shock [e.g., *Luhmann et al*., 1986]. The general lack of strong magnetosonic waves at Mercury implies that the low-frequency magnetic fluctuations in Mercury's magnetosheath are mainly of local sources and not contaminated by the upstream waves. This predicts that Mercury's magnetosheath would be less turbulent than the Earth's magnetosheath. It would be an ideal place to study the waves generic to the magnetosheath.

[38] Finally, we have identified low-frequency waves with distinct spectral peaks at ~ 0.8 Hz (Figures 9 and 10) at Mercury. This type of waves was not reported previously in Mariner 10 data. We have yet to determine if this type of waves is similar to the 3 second upstream waves in the Earth's foreshock [*Le et al*., 1992; *Blanco-Cano et al*., 1999]. The 3 second waves in the Earth's foreshock are found to be always right-handed and nearly circularly polarized in the spacecraft frame. The polarization of the ~ 0.8 Hz waves at Mercury is also found to be right-handed in the spacecraft; and the wave frequency is also consistent with the 3 second waves at the Earth given the high IMF strength at Mercury. In order to draw a conclusion, a statistical survey of this type of waves at Mercury is required.

4. Conclusions

[39] This paper reports our first results of upstream ULF waves in Mercury's foreshock using high time resolution magnetic field data, 20 samples per second, from the MESSENGER spacecraft. Mercury's bow shock is unique in our solar system as it is produced by low Mach number

solar wind blowing over a small magnetized body with a predominately radial interplanetary magnetic field. Our study has showed the existence of at least three types of upstream waves: (1) whistler waves at frequencies near 2 Hz, similar to the 1 Hz waves at the Earth; (2) waves with frequencies ~ 0.3 Hz, similar to the large-amplitude 30 second waves at the Earth; (3) fluctuations with spectral peaks centered at ~ 0.8 Hz. Unlike the Earth's foreshock where the most prominent upstream wave phenomenon is locally generated large-amplitude 30 second magnetosonic waves, the most common foreshock waves are whistler waves generated at the bow shock, with properties similar to the 1 Hz waves in the Earth's foreshock. Their occurrence characteristics show that the "1 Hz" wave generation is generic to the bow shock and not affected by the strength and size of the shock at Mercury. On the other hand, the "30 second" magnetosonic waves at Mercury occur only sporadically and with small amplitudes. The general lack of strong "30 second" magnetosonic waves at Mercury can be attributed to the lack of strong backstreaming ions due to a weak bow shock and not enough time for wave growth due to the small foreshock size. Superposed on the "1 Hz" whistler waves, there are short bursts of spectral peaks at ~ 0.8 Hz that are new and have not been reported previously in Mariner 10 data. The source of the ~ 0.8 Hz waves remains to be identified.

References

Anderson, B. J., M. H. Acuna, D. A. Lohr, J. Scheifele, A. Raval, H. Korth, and J. A. Slavin (2007), The Magnetometer instrument on MESSENGER, *Space Sci. Rev.*, *131*, 417–450, doi:10.1007/s11214-007-9246-7.

Anderson, B. J. et al. (2008), The structure of Mercury's magnetic field from MESSENGER's first flyby, *Science*, *321*, 82–85.

Biskamp, D. (1973), Collisionless shock waves in plasmas, *Nucl. Fusion*, *13*, 719.

Blanco-Cano, X., G. Le, and C. T. Russell (1999), Identification of foreshock waves with 3-s periods, *J. Geophys. Res.*, *104*(A3), 4643–4656, doi:10.1029/1998JA900103.

Blanco-Cano, X., N. Omidi, and C. T. Russell (2006), Macrostructure of collisionless bow shocks: 2. ULF waves in the foreshock and magnetosheath, *J. Geophys. Res.*, *111*, A10205, doi:10.1029/2005JA011421.

Blanco-Cano, X., P. Kajdic, E. Aguilar-Rodriguez, C. T. Russell, L. K. Jian, and J. G. Luhmann (2013), STEREO observations of interplanetary shocks and foreshocks, *Solar Wind 13: Proceedings of the Thirteenth International Solar Wind Conference*, AIP Conf. Proc. 1539, edited by N. V. Pogorelov and G. P. Zank, in press, American Institute of Physics, New York.

Burgess, D., E. Mobius, and M. Scholer (2012), Ion acceleration at the Earth's bow shock, *Space Sci. Rev.*, *173*, 5–47, doi:10.1007/s11214-012-9901-5.

Eastwood, J. P., E. A. Lucek, C. Mazelle, K. Meziane, Y. Narita, J. Pickett, and R. A. Treumann (2005), The foreshock, *Space Sci. Res.*, *118*, 41–94, doi:10.1007/s11214-005-3824-3.

Edmiston, J. P., C. F. Kennel, and D. Eichler (1982), Escape of heated ions upstream of quasi-parallel shocks, *Geophys. Res. Lett.*, *9*(5), 531–534, doi:10.1029/GL009i005p00531.

Fairfield, D. H. (1974), Whistler waves observed upstream from collisionless shocks, *J. Geophys. Res.*, *79*(10), 1368–1378, doi:10.1029/JA079i010p01368.

Fairfield, D. H., and K. W. Behannon (1976), Bow Shock and magnetosheath waves at Mercury, *J. Geophys. Res.*, *81*(22), 3897–3906, doi:10.1029/JA081i022p03897.

Farris, M. H., C. T. Russell, and M. F. Thomsen (1993), Magnetic structure of the low beta, quasi-perpendicular shock, *J. Geophys. Res.*, *98*(A9), doi:10.1029/93JA00958, issn:0148-0227.

Gosling, J. T., and A. E. Robson (1985), Ion reflection, gyration, and dissipation at super-critical shocks, in *Collisionless Shocks in the Heliosphere: Reviews of Current Research*, Geophys. Monogr. Ser., Vol. *35*, edited by B. T. Tsurutani, and R. G. Stone, p. 141, AGU, Washington, DC.

Greenstadt, E. W., and L. W. Baum (1986), Earth's compressional foreshock boundary revisited: observations by ISEE 1 magnetometer, *J. Geophys. Res.*, *91*(A8), 9001.

Greenstadt, E. W., I. M. Green, G. T. Inouye, A. J. Hundhausen, S. J. Bame, and I. B. Strong (1968), Correlated magnetic field and plasma observations of the Earth's bow shock, *J. Geophys. Res.*, *73*(1), 51–60, doi:10.1029/JA073i001p00051.

Hoppe, M. . M., and C. T. Russell (1982), Particle acceleration at planetary bow shock waves, *Nature*, *295*, 41.

Hoppe, M. M., C. T. Russell, L. A. Frank, T. E. Eastman, and E. W. Greenstadt (1981), Upstream hydromagnetic waves and their association with backstreaming ion populations: ISEE 1 and 2 observations, *J. Geophys. Res.*, *86*(A6), 4471–4492, doi:10.1029/JA086iA06p04471.

Hoppe, M. M., C. T. Russell, T. E. Eastman, and L. A. Frank (1982), Characteristics of the ULF waves associated with upstream ion beams, *J. Geophys. Res.*, *87*(A2), 643–650, doi:10.1029/JA087iA02p00643.

Kajdic, P., X. Blanco-Cano, E. Aguilar-Rodriguez, C. T. Russell, L. K. Jian, and J. G. Luhmann (2012), Waves upstream and downstream of interplanetary shocks driven by coronal mass ejections, *J. Geophys. Res.*, *117*, A06103, doi:10.1029/2011JA017381.

Kennel, C. F., J. P. Edmiston, and T. Hada (1985), A quarter century of collisionless shock research, in *Collisionless Shocks in the Heliosphere: A Tutorial Review*, Geophys. Monogr. Ser., vol.*34*, edited by B. T. Tsurutani, and R. G. Stone, p. 1, AGU, Washington, DC.

Kucharek, H., E. Möbius, M. Scholer, C. Mouikis, L. M. Kistler, T. Horbury, A. Balogh, H. Réme, and J. M. Bosqued (2004), On the origin of field-aligned beams at the quasi-perpendicular bow shock: multi-spacecraft observations by Cluster, *Ann. Geophys.*, *22*, 2301–2308, doi:10.5194/angeo-22-2301-2004.

Le, G., and C. T. Russell (1992a), A study of ULF wave foreshock morphology-I. ULF foreshock boundary, *Planet. Space Sci.*, *40*, 1203–1225.

Le, G., and C. T. Russell (1992b), A study of ULF wave foreshock morphology-II. Spatial variation of ULF waves, *Planet. Space Sci.*, *40*, 1227–1234.

Le, G., and C. T. Russell (1996), Solar wind control of upstream wave frequency, *J. Geophys. Res.*, *101*(A2), 2571–2575, doi:10.1029/95JA03151.

Le, G., C. T. Russell, M. F. Thomsen, and J. T. Gosling (1992), Observations of a new class of upstream waves with periods near 3 seconds, *J. Geophys. Res.*, *97*(A3), 2917–2925, doi:10.1029/91JA02707.

Lucek, E. A., and A. Balogh (1997), Ulysses observations of a discrete wavepacket upstream of an interplanetary shock, *Geophys. Res. Lett.*, *24*(19), 2387–2390, doi:10.1029/97GL52471.

Luhmann, J. G., C. T. Russell, and R. C. Elphic (1986), Spatial distributions of magnetic field fluctuations in the dayside magnetosheath, *J. Geophys. Res.*, *91*(A2), 1711–1715, doi:10.1029/JA091iA02p01711.

Ness, N. F., K. W. Behannon, R. P. Lepping, and Y. C. Whang (1975), The magnetic field of Mercury, 1, *J. Geophys. Res.*, *80*(19), 2708–2716, doi:10.1029/JA080i019p02708.

Omidi, N., and D. Winske (1990), Steepening of kinetic magnetosonic waves into shocklets: Simulations and consequences for planetary shocks and comets, *J. Geophys. Res.*, *95*(A3), 2281–2300, doi:10.1029/JA095iA03p02281.

Omidi, N., X. Blanco-Cano, and C. T. Russell (2005), Macrostructure of collisionless bow shocks: 1. Scale lengths, *J. Geophys. Res.*, *110*, A12212, doi:10.1029/2005JA011169.

Orlowski, D. S., and C. T. Russell (1991), ULF waves upstream of the Venus bow shock: Properties of one-hertz waves, *J. Geophys. Res.*, *96*(A7), 11,271–11,282, doi:10.1029/91JA01103.

Orlowski, D. S., G. K. Crawford, and C. R. Russell (1990), Upstream waves at mercury, Venus and earth: Comparison of the properties of one Hertz waves, *Geophys. Res. Lett.*, *17*(13), 2293–2296, doi:10.1029/GL017i013p02293.

Orlowski, D. S., C. T. Russell, and D. Krauss-Varban (1993), On the source of upstream whistlers in the Venus foreshock, in *Plasma Environments of Non-Magnetic Planets*, edited by Pergamon Press, New York, pp. 217–227 .

Orlowski, D. S., C. T. Russell, D. Krauss-Varban, N. Omidi, and M. F. Thomsen (1995), Damping and spectral formation of upstream whistlers, *J. Geophys. Res.*, *100*(A9), 17,117–17,128, doi:10.1029/95JA00062.

Paschmann, G., N. Sckopke, J. R. Asbridge, S. J. Bame, and J. T. Gosling (1980), Energization of solar wind ions by reflection from the Earth's bow shock, *J. Geophys. Res.*, *85*(A9), 4689–4693, doi:10.1029/JA085iA09p04689.

Russell, C. T. (1994), Planetary upstream waves, in *Solar Wind Sources of Magnetospheric Ultra-Low-Frequency Waves*, Geophys. Monogr. Ser., vol. *81*, edited by M. J. Engebreston, K. Takahashi, and M. Scholer, pp. 75–86, AGU, Washington, D. C., doi:10.1029/GM081p0075.

Russell, C. T. (2007), Upstream whistler-mode waves at planetary bow shocks: A brief review, *Atmos. Sol-Terr. Phys.*, *69*, 1739–1746.

Russell, C. T., D. N. Baker, and J. A. Slavin (1988), The magnetosphere of Mercury, in *Mercury*, edited by F. Vilas, C. R. Chapman, and M. S. Matthews, pp. 514–61, University of Arizona Press, Tucson.

Russell, C. T., L. K. Jian, X. Blanco Cano, J. G. Luhmann, and T. L. Zhang (2009), STEREO observations of shock formation in the solar wind, *Geophys. Res. Lett.*, *36*, L02103, doi:10.1029/2008GL036337.

Schwartz, S. J., D. Burgess, and J. J. Moses (1996), Low-frequency waves in the Earth's magnetosheath: Present status, *Ann. Geophys.*, *14*, 1134–1150.

Sckopke, N., G. Paschmann, A. L. Brinca, C. W. Carlson, and H. Lühr (1990), Ion thermalization in quasi-perpendicular shocks involving reflected ions, *J. Geophys. Res.*, *95*(A5), 6337–6352, doi:10.1029/JA095iA05p06337.

Slavin, J. A., and R. E. Holzer (1981), Solar wind flow about the terrestrial planets 1. Modeling bow shock position and shape, *J. Geophys. Res.*, *86*(A13), 11,401–11,418, doi:10.1029/JA086iA13p11401.

Slavin, J. A., et al. (2009), MESSENGER observations of Mercury's magnetosphere during northward IMF, *Geophys. Res. Lett.*, *36*, L02101, doi:10.1029/2008GL036158.

Sonnerup, B. U. Ö. (1969), Acceleration of particles reflected at a shock front, *J. Geophys. Res.*, *74*(5), 1301–1304, doi:10.1029/JA074i005p01301.

Sonnerup, B. U. Ö., and L. J. Cahill Jr. (1967), Magnetopause structure and attitude from Explorer 12 observations, *J. Geophys. Res.*, *72*(1), 171–183, doi:10.1029/JZ072i001p00171.

Sundkvist, D., V. Krasnoselskikh, S. D. Bale, S. J. Schwartz, J. Soucek, and F. Mozer (2012), Dispersive nature of high Mach number collisionless plasma shocks: Poynting flux of oblique whistler waves, *Phys. Rev. Lett.*, *108*, 025002, doi:10.1103/PhysRevLett.108.025002.

Swanson, D. G. (2003), Plasma Waves, in *Series in Plasma Physics*, Taylor Francis Ltd, United Kingdom, 2nd edition, pp. 62 .

Tanaka, M., C. C. Goodrich, D. Winske, and K. Papadopoulos (1983), A source of the backstreaming ion beams in the foreshock region, *J. Geophys. Res.*, *88*(A4), 3046–3054, doi:10.1029/JA088iA04p03046.

Thomsen, M. F., S. J. Schwartz, and J. T. Gosling (1983), Observational evidence on the origin of ions upstream of the Earth's bow shock, *J. Geophys. Res.*, *88*(A10), 7843–7852, doi:10.1029/JA088iA10p07843.

Thomsen, M. F., J. T. Gosling, S. J. Bame, and M. M. Mellott (1985), Ion and electron heating at collisionless shocks near the critical Mach number, *J. Geophys. Res.*, *90*(A1), 137–148, doi:10.1029/JA090iA01p00137.

Thomsen, M. F., J. T. Gosling, T. G. Onsager, and C. T. Russell (1993), Ion and electron heating at the low-Mach-number, quasi-parallel bow shock, *J. Geophys. Res.*, *98*(A3), 3875–3888, doi:10.1029/92JA02560.

Wilson, L. B., III, C. A. Cattell, P. J. Kellogg, K. Goetz, K. Kersten, J. C. Kasper, A. Szabo, and K. Meziane (2009), Low-frequency whistler waves and shocklets observed at quasi-perpendicular interplanetary shocks, *J. Geophys. Res.*, *114*, A10106, doi:10.1029/2009JA014376.